LETTER Communicated by Geoffrey Goodhill

An Analysis of Orientation and Ocular Dominance Patterns in the Visual Cortex of Cats and Ferrets

T. Müller
M. Stetter
Department of Computer Science, TU Berlin, 10587 Berlin, Germany

M. Hübener
F. Sengpiel
T. Bonhoeffer
Max-Planck-Institute of Neurobiology, 82152 Martinsried, Germany

I. Gödecke
Actipac Biosystems GmbH, 82152 Martinsried, Germany

B. Chapman
Davis Center for Neuroscience, UC Davis, Davis, CA 95616 U.S.A.

S. Löwel
Leibniz-Institut für Neurobiologie, 39118, Magdeburg, Germany

K. Obermayer
Department for Computer Science, TU Berlin, 10587 Berlin, Germany

We report an analysis of orientation and ocular dominance maps that were recorded optically from area 17 of cats and ferrets. Similar to a recent study performed in primates (Obermayer & Blasdel, 1997), we find that 80% (for cats and ferrets) of orientation singularities that are nearest neighbors have opposite sign and that the spatial distribution of singularities deviates from a random distribution of points, because the average distances between nearest neighbors are significantly larger than expected for a random distribution. Orientation maps of normally raised cats and ferrets show approximately the same typical wavelength; however, the density of singularities is higher in ferrets than in cats. Also, we find the well-known overrepresentation of cardinal versus oblique orientations in young ferrets (Chapman & Bonhoeffer, 1998; Coppola, White, Fitzpatrick, & Purves, 1998) but only a weak, not quite significant overrepresentation of cardinal orientations in cats, as has been reported previously (Bonhoeffer & Grinvald, 1993). Orientation and ocular dominance slabs in cats exhibit a tendency of being orthogonal to each other (Hübener, Shoham, Grinvald, & Bonhoeffer, 1997), albeit less pronounced, as has been re-

ported for primates (Obermayer & Blasdel, 1993). In chronic recordings from single animals, a decrease of the singularity density and an increase of the ocular dominance wavelength with age but no change of the orientation wavelengths were found.

Orientation maps are compared with two pattern models for orientation preference maps: bandpass-filtered white noise and the field analogy model. Bandpass-filtered white noise predicts sign correlations between orientation singularities, but the correlations are significantly stronger (87% opposite sign pairs) than what we have found in the data. Also, bandpass-filtered noise predicts a deviation of the spatial distribution of singularities from a random dot pattern. The field analogy model can account for the structure of certain local patches but not for the whole orientation map. Differences between the predictions of the field analogy model and experimental data are smaller than what has been reported for primates (Obermayer & Blasdel, 1997), which can be explained by the smaller size of the imaged areas in cats and ferrets.

1 Introduction

In a previous study (Obermayer & Blasdel, 1997), we analyzed orientation and ocular dominance maps obtained from the striate cortex of macaque and squirrel monkeys. We found a strong correlation between the properties and locations of orientation singularities, and we also found that this and several other properties of those maps can be well described by their second-order statistics. The spatial structure of the maps was fairly similar across animals, species, and ages for the measures used, except for a different overall alignment of orientation bands and different periods of repetition.

Here we report a follow-up study using data from cats and ferrets, whose visual pathways differ from primates by a set of distinct features—for example the number of primary visual areas receiving strong, direct geniculate input and the distribution of cells with different response properties over the different cortical layers. Both species show ocular dominance (LeVay, Stryker, & Shatz, 1978; Anderson, Olavarria, & Sluyters, 1988; Redies, Diksic, & Riml, 1990), albeit less pronounced than in macaque striate cortex. Ferrets and cats additionally exhibit clusters of strongly direction-selective cells in the upper layers (Shmuel & Grinvald, 1996; Weliky, Bosking, & Fitzpatrick, 1996), which could, in principle, interact with the spatial layout of orientation-selective cells. Our analysis was performed on 51 orientation and 10 ocular dominance maps obtained from 21 animals, including maps from chronic recordings in single animals over age (longitudinal studies) (Gödecke & Bonhoeffer, 1996), and maps from animals raised under strabismus (Sengpiel et al., 1998). The results are compared with two pattern models: (1) bandpass-filtered white noise (Swindale, 1982; Rojer & Schwartz, 1990; Cowan & Friedman, 1991; Shvartsman & Freund, 1994), which assumes that orientation maps can be fully described by their second-order

statistics, and (2) the field analogy model (Wolf, Pawelzik, & Geisel, 1994; Wolf, Pawelzik, Geisel, Kim, & Bonhoeffer, 1994), which claims that orientation maps are optimally smooth given the locations and signs of their singularities.

The letter is divided into five sections. In section 2 we describe the data and the methods for data analysis. In the third section, we briefly introduce both pattern models. The fourth section contains the results of our data analysis and our comparison between data and models, and the fifth section concludes with a brief discussion.

2 Data and Methods of Analysis

2.1 Data Collection and Preprocessing. The data were obtained by optical recording of intrinsic signals (Blasdel, 1992) using standard procedures (Bonhoeffer & Grinvald, 1996), but using light wavelength of 707 nm for the illumination of the cortex. For the purpose of this article, each "raw" data set consists of 16 × 5 frames, 192 × 144 pixels in size, with a 2-byte number representing the pixel's intensity as recorded by the CCD camera. One stimulus condition corresponds to a block of five frames covering a time window of 3 s (600 ms per frame), which are recorded during stimulation of the animal. Stimuli are bar gratings of four orientations (0, 45, 90, and 135 degrees), which are presented four times each, giving rise to the 16 blocks of frames. Each stimulation is preceded by a 7 s presentation of a static bar grating, which is then moved for 3 s to form the actual stimulus. Afterwards, another randomly selected static bar grating is presented to prepare the next stimulation. If, in addition, ocular dominance is measured, eight conditions are presented only to the right and the other 8 conditions only to the left eye, respectively.

Every block of five frames was processed by subtraction of the first captured frame from the four subsequent ones (first frame analysis) and by normalization using a cocktail blank, as described in Bonhoeffer and Grinvald (1996), followed by a pixel-by-pixel average over frames 2 to 5. For the case of ocular dominance, difference images D_{OD} were generated by first averaging the frames for all left eye and right eye presentations separately and then subtracting the right eye average from the left eye average pixel by pixel. For the case of orientation selectivity, two difference images were obtained by first averaging all frames recorded during the presentations of an oriented grating independent of eye, and then subtracting the 90 degrees (135 degrees) from the 0 degrees (45 degrees) average pixel by pixel, generating the orientation difference image D_{OR}^{0-90} (D_{OR}^{45-135}).

Animals that had large blood vessel artifacts running across the recorded area and experiments with a weak signal were excluded by visual inspection of the maps and the blood vessel patterns. This procedure yielded 52 out of the 221 data sets. For each of the remaining images, a region of interest was

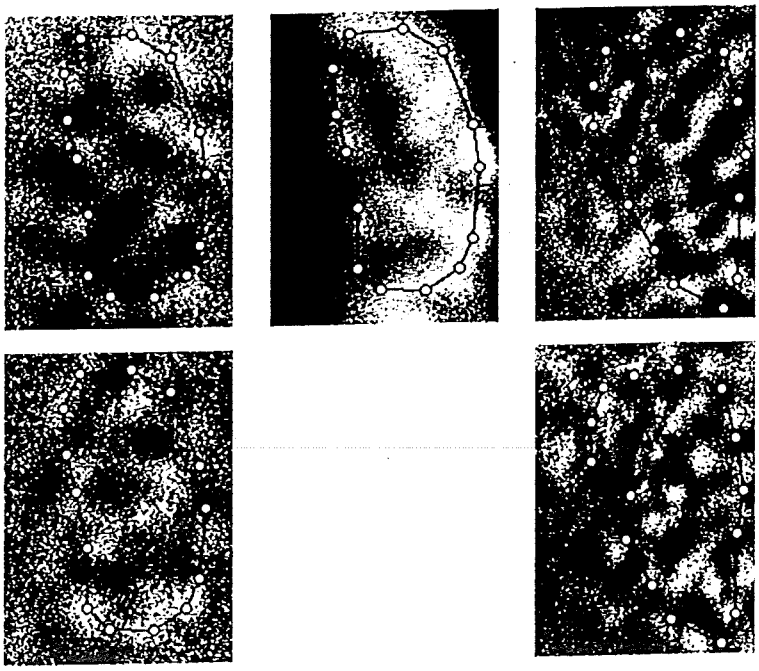

Figure 1: (Left) Differential maps for orientation (0–90 degrees, top; 45–135 degrees, bottom) of a cat (experiment C10b). (Middle) Ocular dominance map of the same experiment (C10b). (Right) Differential maps for orientation (0–90 degrees, top; 45–135 degrees, bottom) of a ferret (experiment F1a). The polygons specify the corresponding regions of interest before reduction in size.

drawn, which outlined a zone that avoids artifacts (see Figure 1). For the analysis, these regions of interest were reduced further by 30% in diameter in order to exclude pixels near the boundary that could be affected by artifacts.

Table 1 summarizes the data sets used in our study, together with the animals age, the size of the region of interest, estimates of the orientation and ocular dominance wavelengths, and an estimate of the mean and maximum signal-to-noise ratio of the difference images as a measure of data quality (see section 2.2).

In order to enhance the signal-to-noise ratio of the difference images, a bandpass filter B,

$$B(\vec{k}) = \sigma\left(\frac{2\pi}{\lambda_{\text{high}}} - |\vec{k}|\right)\ \sigma\left(|\vec{k}| - \frac{2\pi}{\lambda_{\text{low}}}\right), \tag{2.1}$$

is applied to the difference images in Fourier space, where $\vec{k}$ is the wave vector and $\sigma(x)$,

$$\sigma(x) = \frac{1}{1+\exp(-\beta x)}, \tag{2.2}$$

Table 1: Summary of Data Sets Analyzed.

Ferret	Age (d)	m/σ mean	m/σ max	ROI (mm^2)	λ_{OR} (mm)	Cat	Age (d)	m/σ mean	m/σ max	ROI (mm^2)	λ_{OR} (mm)	λ_{OD} [mm]
F1a*	38	0.46	1.77	5.32	0.64	C1*	32	0.44	2.96	6.18	0.87	—
F1b	38	0.50	3.54	9.81	0.71	C2	65	0.31	2.25	11.43	0.83	—
F1c	43	0.58	2.52	17.64	0.73	C3	60	0.31	4.21	45.44	0.92	—
F1d	56	0.27	0.83	9.81	0.76	C4a	60	0.58	2.52	9.81	0.72	—
F2a	44	0.55	1.79	10.13	0.73	C4b*	60	0.31	1.97	7.95	0.76	—
F2b	47	0.62	1.89	34.80	0.71	C5*	50	0.36	3.39	15.02	0.63	—
F3a	35	0.82	2.52	13.40	0.68	C6*	50	0.30	1.12	7.51	0.65	—
F3b	39	0.69	1.69	13.40	0.69	C7a	54	0.29	2.94	32.12	0.72	—
F3c	42	0.57	1.74	13.40	0.7	C7b	54	0.46	1.64	9.55	0.72	0.83
F4a	37	0.71	2.06	23.84	0.81	C8a	52	0.42	1.54	30.74	0.71	—
F4b	39	0.57	1.85	23.84	0.74	C8b	52	0.47	1.63	15.37	0.71	0.76
F4c	42	0.65	1.79	23.84	0.78	C9	54	0.40	3.32	22.72	0.91	—
F5a	40	0.63	1.75	18.12	0.7	C10a*	50	0.43	1.75	9.58	0.72	—
F5b	43	0.54	1.72	18.12	0.65	C10b*	50	0.65	2.05	5.17	0.67	1.04
F6a	38	0.71	1.99	19.46	0.71	CS1a	27	0.27	6.20	8.10	0.75	0.65
F6b	41	0.67	1.65	19.46	0.68	CS1b	34	0.53	4.29	8.10	0.74	0.79
F7*	100	0.70	1.82	7.20	0.63	CS1c	42	0.41	10.63	8.10	0.78	0.8
F8	41	0.50	1.70	19.48	0.67	SC1d	54	0.36	10.37	8.10	0.67	0.73
F9a	38	0.68	3.65	16.82	0.63	CS1e	61	0.41	6.71	2.24	0.8	1.02
F9b	41	0.62	2.19	16.82	0.74	CS2a	27	0.68	2.61	17.27	0.75	1.03
F9c	44	0.72	1.84	16.82	0.66	CS2b*	38	0.37	2.00	6.08	0.61	0.73
F9d*	118	0.46	1.52	7.60	0.61							

Notes: The columns on the left show ferret (F) data; the columns on the right show data recorded from normal (C) and strabismic (CS) cats. Numbers within the names denote different animals; letters at the names' end indicate different recordings from the same animal and cortical area. Mean ($(m/\sigma)_{mean}$) and maximum ($(m/\sigma)_{max}$) signal-to-noise ratios, orientation wavelengths (λ_{OR}), and ocular dominance wavelengths (λ_{OD}) are measured as described in section 2.2. The region of interest (ROI) column lists the size of the cortical areas used for evaluation. Asterisks indicate animals, which are recorded with higher resolution. Note that ocular dominance was recorded only in some of the experiments with cats, including normal and strabismic animals. Data with large regions of interest represent means over several experiments. Some of the data were already used in other publications.

is the logistic function. The bandpass filter is designed to reduce the high spatial frequency noise induced by the imaging process (photon shot noise and camera noise) as well as the low spatial frequency biological noise (blood volume components, hemodynamics). Parameters were chosen: $\lambda_{high} = 0.25$ mm, $\lambda_{low} = 2.0$ mm, and $\beta = 1.4$ mm. In the following, spatially filtered images are used unless otherwise noted.

The orientation difference images D_{OR}^{0-90} and D_{OR}^{45-135} are sometimes combined to form the real and imaginary components of a complex orientation field $O(\vec{r})$ (Swindale, 1982),

$$O(\vec{r}) = D_{OR}^{0-90}(\vec{r}) + iD_{OR}^{45-135}(\vec{r}), \tag{2.3}$$

where i is the imaginary unit. Using polar coordinates,

$$O(\vec{r}) = q(\vec{r}) \exp(2i\phi(\vec{r})), \tag{2.4}$$

one then obtains a measure for the preferred orientation, $\phi(\vec{r})$, and the orientation tuning strength, $q(\vec{r})$, as a function of cortical location (Blasdel & Salama, 1986).

Figure 1 shows typical examples of an orientation map (Figure 1a) and an ocular dominance map (Figure 1b) of a cat and an orientation map of a ferret (Figure 1c).

2.2 Signal-to-Noise Ratios, Wavelengths, and Gradients. In order to obtain an estimate of the signal-to-noise ratio for the high-frequency photon shot noise as well as camera noise, every image is divided into blocks of 3×3 pixels. Mean values m and standard deviations σ of pixel values are calculated for every block, and the ratio m/σ is averaged over all blocks within the region of interest to form the mean signal-to-noise ratio $(m/\sigma)_{mean}$, whereas $(m/\sigma)_{max}$ stores the maximum of the ratio.

The typical wavelengths of the orientation and ocular dominance maps are determined by first computing the spatial power spectra of the unfiltered difference image D_{OD} and the unfiltered complex orientation map O, equation 2.3, using a fast fourier transformation. The power of all modes of similar wave number $|\vec{k}|$ is added, and the wave numbers $|\vec{k}_{OR/OD}|$ of the peaks of the summed spectra are determined. The wavelengths $\lambda_{OR/OD}$ are then calculated from $\lambda_{OR/OD} = 2\pi/|\vec{k}_{OR/OD}|$.

Gradients from difference images are estimated by fitting a plane $D = a + bx + cy$ to the pixel values of a 3×3 size region (least squares fit; Spiegel, 1975). The parameters a, b, and c are then given by:

$$a = \frac{\sum_j D_j}{9}, \quad b = \frac{\sum_j x_j D_j}{6}, \quad c = \frac{\sum_j y_j D_j}{6}, \tag{2.5}$$

where j runs over all pixels in the 3×3 region and (x_j, y_j) are their spatial coordinates. The gradient, ∇D, at the center pixel is then given by

$$\nabla D = (b\ c)^T. \tag{2.6}$$

Gradients of orientation preference angles are calculated in a similar fashion, except that D is replaced by the difference of the orientation angle at the considered pixel location and the orientation angle at the center pixel, corrected by multiples of π if necessary.

2.3 Positions and Signs of Orientation Singularities. Singularities in orientation maps correspond to the zeroes of the function $O(\vec{r})$. When linearized, the orientation field around a singularity can be described by the location of the zero crossing and the four additional parameters: amplitude, anisotropy, angle, and skewness (for details see Obermayer & Blasdel, 1997). The sign of a singularity is then given by the sign of its amplitude parameter. It is positive if orientation preferences increase in a clockwise direction around the singularity, and negative otherwise.

In order to determine the position of singularities in the experimental data, changes of orientation preferences are added clockwise along small circles of radius 70 μm around every pixel in the image. If the sum along a closed loop is close to $\pm\pi$ (difference less than 10^{-6}), then a singularity is enclosed by the circle and the pixel is marked by either $+1$ or -1 depending on the sign of the enclosed singularity. Otherwise the pixel is marked by 0. Ideally, after this procedure, each singularity in the data is covered by a patch with radius 70 μm of pixels marked by ± 1, which is surrounded by pixels marked with 0. Disks of radius 70 μm are then fitted to the regions marked $+1$ and -1. The position of the singularity is then given by the location of the center of a disk with maximum overlap with the corresponding region (best fit). We ignored regions with less than 33% overlap.

3 Models

3.1 Surrogate Data. We consider the hypothesis that the spatial patterns of orientation and ocular dominance can be fully described by their second-order statistics—that is, their power spectrum—but are otherwise random. If the power spectrum is taken from experimentally measured maps, so-called surrogate data maps can be generated by randomizing the phases of the individual Fourier modes in the maps' Fourier spectra. Let $\tilde{D}(\vec{k})$ be the experimentally measured Fourier spectrum of a difference map $D(\vec{r})$, and let $\chi(\vec{k})$ be a random number from the interval $[0, 2\pi]$. A surrogate data map $\hat{SD}$ is then calculated by

$$\hat{SD} = \mathcal{F}^{-1}\left(|\tilde{D}(\vec{k})| \exp\{i\chi(\vec{k})\}\right). \tag{3.1}$$

In order to generate surrogate data for orientation preference maps, one has to take into account that both orientation difference maps, D_{OR}^{0-90} and D_{OR}^{45-135}, are coupled because they are generated by the orientation tuning curve of the same neurons. This implies that the phase relationship between both difference maps must be preserved; hence, phases must be randomized with respect to the Fourier spectrum $\tilde{O}(\vec{k})$ of the complex orientation map $O(\vec{r})$—that is, $\tilde{D}(\vec{k})$ has to be replaced by $\tilde{O}(\vec{k})$ in equation 3.1. Surrogate data maps, 192 × 144 pixels in size, were generated for each data set until the total number of singularities in all surrogate data maps was at least 10^5 for every experimental map. Note that the above method to generate surrogate data is similar to the method of generating maps from bandpass-filtered noise models (Swindale, 1982; Rojer & Schwartz, 1990; Cowan & Friedman, 1991; Niebur & Wörgötter, 1994; Freund, 1994; Shvartsman & Freund, 1994; Schwartz, 1994; Erwin, Obermayer, & Schulten, 1995).

3.2 The Field Analogy Model. The field analogy model (FAM) (Wolf, Pawelzik, & Geisel, 1994; Wolf, Pawelzik, Geisel, Kim, & Bonhoeffer, 1994) is a pattern model that explains the spatial pattern of orientation maps by two underlying principles: (1) that the orientation map is fully determined by the locations $\{x_j, y_j\}$ and signs $\{v_j\}$ of the singularities and (2) that the orientation map in between those singularities is optimally smooth. For every given set of locations and signs of singularities, an orientation map $\Psi(x, y)$ can be calculated as

$$\Psi(x,y) = \arg\left(\prod_j \{(x-x_j) - iv_j(y-y_j)\}\right) = \arg\left(\prod_j O_j\right), \quad (3.2)$$

which defines the FAM model.

In order to test the FAM approach, locations and signs of singularities are determined from the experimental data, and the orientation map is reconstructed using equation 3.2. The error R between the original map $\Theta(x, y)$ and its reconstruction $\Psi(x, y)$ is calculated by

$$R^2 = \frac{1}{N}\sum_{x,y}\{g(\Psi(x,y) - \Theta(x,y) + \Theta_{\text{ref}})\}^2, \quad (3.3)$$

where (x, y) are pixel locations, N is the number of pixels in the sum, Ψ is given by equation 3.2, Θ denotes the original orientation preference, and Θ_{ref} is chosen such that R is minimal. The function g is given by

$$g(\phi) = \begin{cases} \phi + \pi & \text{if } \phi < -\pi/2 \\ \phi & \text{if } -\pi/2 \le \phi < \pi/2 \\ \phi - \pi & \text{if } \phi \ge \pi/2 \end{cases}. \quad (3.4)$$

In order to avoid boundary effects, the maximum region of interest for the determination of the reconstruction error via equation 3.3 is 30% smaller in area than the original region of interest from Table 1.

4 Results

4.1 Distribution of Orientation Preferences. In the ferret, orientation maps consistently show an overrepresentation in area for orientation preferences close to 0 and 90 degrees (Chapman & Bonhoeffer, 1998). A significance test for this overrepresentation is not easy to perform because orientations of adjacent pixels are generally not statistically independent. Dependencies arise because of structure in the orientation map and a blur of the signal caused by light scattering in the tissue (Stetter & Obermayer, 1999). In order to avoid correlations due to tissue scattering, the orientation values were subsampled such that their distance exceeded the correlation length of about 100 μm (Bonhoeffer & Grinvald, 1996) caused by the blur. For the test, orientation values were sampled at the inverse Nyquist frequency of the low-pass-filtered images (125 μm).

Figure 2 (left) shows a histogram of the percentage of pixels as a function of orientation preference for a typical example (ferret F2a). Angles are pooled into 12 bins of size 15 degrees and compared to the hypothesis that all orientation angles occur equally often. The deviation from uniformity is significant for all but three ferret data from Table 1 (χ^2 test, significance level of mean histogram: $34.1 > 19.7, \alpha = 0.05$). We also calculated the fractions of cortical area showing orientation preferences between 157.5 and 22.5 degrees and between 67.5 and 112.5 degrees. Typically, these cardinal-like orientations were found to occupy a fraction of 60% of the total area of the orientation map (compared to 50% expected for a random distribution). In some of the ferret data sets, it can be shown that the overrepresentation is largest shortly after eye opening (cf. Chapman & Bonhoeffer, 1998).

In the cat, only a weak tendency for preference of cardinal orientations can be observed. Some sets of data show an overrepresentation of angles close to 0 and 90 degrees; others show overrepresentation of obliques, and for some, sets of data orientations are equally represented. Correspondingly, all but six cat orientation histograms are significantly nonuniform, yet with smaller significance levels than ferret data. Moreover, the mean histogram does not significantly differ from uniformity (significance level $15.8 < 19.7$, $\alpha = 0.05$).

Close to the border between areas 17 and 18 the cortical maps are arranged in an ordered way with respect to the border line (Chapman, Stryker, & Bonhoeffer, 1996). We tested whether the preference for cardinal orientations is related to the proximity to the 17/18 border, as well by subdividing the regions of interest for all data sets into a lateral and a medial part of equal size, resulting in two parts near and far from the 17/18 bor-

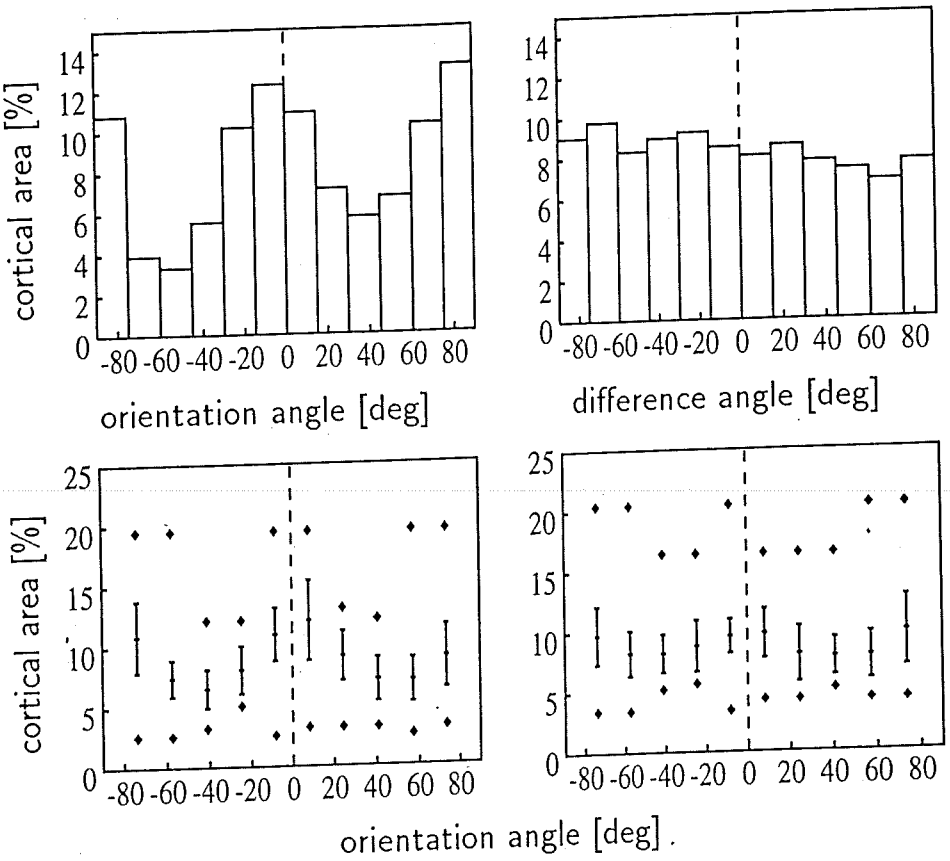

Figure 2: Percentage of cortical area within the ROI as a function of its orientation preference (upper left) and of the angle between the preferred orientation and the local orientation gradient (upper right) for ferret F2. The lower two plots show average distribution of orientation preference as error bars (2σ range) for ferrets (left) and cats (right). The diamonds above and below the error bars denote the minimum and maximum values found in our data.

der. The orientation histograms for both subdivisions were calculated for each animal, and the hypothesis that both histograms are drawn from the same distribution was tested on both the individual histograms and the histograms summed over all cats and all ferrets within each subdivision. The hypothesis could not be rejected in either case, and the extremely low significance values (summed histograms: $\chi^2 = 0.4 < 25, \alpha = 0.05$ for cats, $\chi^2 = 1.28 < 23.7, \alpha = 0.05$ for ferrets) showed that the histograms were very similar to each other. This suggests that the preference for cardinal orientations is not evoked by the proximity to the 17/18 border. However, the cortical areas examined represent only a small fraction of area 17 and do not contain parts very far from the border, which could contribute to the lack of significance.

Figure 2 (right) shows a histogram of the number of pixels as a function of the angle between the preferred orientation at a spatial location and the local orientation gradient for a typical data set (ferret F2). No significant correlations between the preferred orientation and the direction of the iso-orientation lines have been observed for the data sets of Table 1 or for the corresponding surrogate data maps. This finding is similar to what has been reported for macaque striate cortex (Obermayer & Blasdel, 1993).

The average wavelength of the orientation pattern is 0.70 ± 0.01 mm for ferrets and 0.75 ± 0.03 mm for cats (see Table 1). Table 2 shows the density of singularities for all data sets listed in Table 1. The density of singularities was found to be (4.5 ± 0.2) mm^{-2} for ferrets and (3.5 ± 0.2) mm^{-2} for cats with ages between 50 and 61 days (error values are the standard error of the mean).

Changes with age have been tested in a longitudinal study on the strabismic kitten CS1. For this animal, the singularity density was found to decrease significantly with age—the decrease rate being 2.1% per day (correlation coefficient $r = -0.88$). However, no significant change of the orientation wavelength with age could be detected (correlation coefficient $r = 0.03$) for this particular animal.

4.2 Correlations Between Locations and Signs of Singularities. Table 2 shows the percentages of nearest-neighbor pairs that have same and opposite signs. On average, $19.7\% \pm 1.5\%$ (ferrets), $21.4\% \pm 2.0\%$ (normal cats), and $22\% \pm$ (strabismic cats) pairs of singularities are of equal sign, where error margins denote the standard deviation of the mean. This has to be compared with the values for the surrogate data model (between $13.6\% \pm 0.2\%$ and $12.4\% \pm 0.3\%$), which are significantly lower. The numbers increase for the second nearest neighbors ($\approx 40\%$) and approach 50% for singularities further apart (data not shown). No significant tendencies have been observed with age or raising conditions.

Figure 3 shows a typical histogram of the distances between singularities that are nearest neighbors, independent of sign. The results for the experimental maps are compared to the results for surrogate data (SD) and a random distribution of points in the plane (RAN). Let ρ be the number density of points and $\Delta = 1/\sqrt{\rho}$ be the square root of the average area per point. The probability density $P(d)$ of distances d between nearest neighbors is then given by the Rayleigh distribution (Papoulis, 1965)

$$P(d) = 2\pi \frac{d}{\Delta} \exp\left\{-\pi \left(\frac{d}{\Delta}\right)^2\right\}. \tag{4.1}$$

Figure 3 shows that the peak of the experimental distribution under consideration of all pinwheel pairs is slightly shifted toward larger values compared to equation 4.1, with the average shift being 0.03Δ for both cats

Table 2: Number Densities and Sign Statistics of Singularities for All Data Sets Listed in Table 1 and the Corresponding Surrogate Data (SD).

Name			OR			SD			Name			OR			SD		
	#± / #+	$\overline{\delta}$ / $[\frac{\#}{mm^2}]$	++% / +−%	−−% / −+%	$\sum$ / $\sum$	++% / +−%	−−% / −+%	$\sum$ / $\sum$		#± / #+	$\overline{\delta}$ / $[\frac{\#}{mm^2}]$	++% / +−%	−−% / −+%	$\sum$ / $\sum$	++% / +−%	−−% / −+%	$\sum$ / $\sum$
F1a	42	7.89	10	3	13	6	6	12	C1	22	3.56	0	13	13	5	6	11
	20		42	45	87	44	44	88		9		38	50	88	45	44	89
F1b	44	4.48	14	19	32	6	7	13	C2	23	2.01	6	6	12	6	6	12
	21		32	35	68	43	43	87		13		47	41	88	44	44	88
F1c	74	4.20	24	14	38	7	7	14	C3	136	3.10	15	11	26	7	7	14
	42		35	27	62	43	43	86		72		42	32	74	43	43	86
F1d	39	3.97	3	12	15	7	7	15	C4a	41	4.18	16	19	35	7	7	14
	20		42	42	85	43	43	85		21		39	26	65	43	43	86
F2a	41	4.05	14	3	17	7	7	14	C4b	37	4.66	0	15	15	6	6	12
	21		39	44	83	43	43	86		20		44	41	85	44	44	88
F2b	115	3.31	8	12	20	7	7	14	C5	59	3.93	13	0	13	5	6	11
	62		42	38	80	43	43	86		31		44	43	87	45	44	89
F3a	75	5.6	5	11	15	6	7	13	C6	23	3.06	0	5	5	7	6	13
	41		47	38	85	43	43	87		11		45	50	95	43	44	87
F3b	59	4.41	10	8	17	6	7	13	C7	106	3.30	10	10	20	7	7	14
	31		42	40	83	43	44	87		51		39	41	80	43	43	86
F3c	48	3.58	21	5	26	6	6	13	C8a	107	3.48	10	13	23	7	6	13
	29		44	31	74	44	43	87		56		40	37	77	43	44	87
F4a	125	5.24	8	10	18	6	6	12	C8b	44	2.86	13	5	18	6	6	13
	63		43	39	82	44	44	88		25		45	38	83	43	44	87
F4b	108	4.53	13	8	20	7	7	13	C9	71	3.14	8	6	14	6	7	13
	56		39	41	80	43	44	87		35		44	42	86	44	43	87
F4c	116	4.87	14	6	20	6	7	13	C10a	36	3.82	10	3	14	7	6	12
	63		39	40	80	43	43	87		19		41	45	86	43	44	88

Table 2: Continued.

Name	#± / #+	$\bar{\delta}$ [$\frac{\#}{mm^2}$]	OR ++% / +−%	OR −−% / −+%	OR $\sum\sum$	SD ++% / +−%	SD −−% / −+%	SD $\sum\sum$	Name	#± / #+	$\bar{\delta}$ [$\frac{\#}{mm^2}$]	OR ++% / +−%	OR −−% / −+%	OR $\sum\sum$	SD ++% / +−%	SD −−% / −+%	SD $\sum\sum$
F5a	69	3.84	17	8	25	8	8	15	C10b	25	4.83	17	42	58	6	6	12
	36		37	38	75	42	42	85		12		25	17	42	44	44	88
F5b	77	4.29	19	11	30	7	7	14	CS1a	48	5.93	12	5	17	6	6	12
	41		34	36	70	43	43	86		26		44	39	83	44	44	88
F6a	96	4.95	14	7	21	6	6	12	CS1b	49	6.05	10	4	14	6	6	12
	52		41	38	79	44	44	88		27		45	41	86	44	44	88
F6b	85	4.39	5	11	16	7	7	13	CS1c	28	3.46	17	22	39	7	6	13
	39		41	43	84	43	43	87		14		30	30	61	43	43	87
F7	39	5.43	6	16	23	6	6	12	CS1d	28	3.46	13	9	22	7	7 14	
	19		42	35	77	44	44	88		14		30	48	78	43	43	86
F8	71	3.71	9	8	17	7	7	14	CS1e	7	3.13	0	0	0	7	6	13
	35		39	44	83	43	43	86		3		40	60	100	43	44	87
F9a	77	4.61	9	13	22	6	6	13	CS2a	88	5.1	21	6	27	6	6	13
	38		42	36	78	44	44	87		49		36	37	73	43	44	87
F9b	69	4.13	2	8	10	7	7	14	CS2b	52	8.6	9	9	17	5	6	11
	32		44	46	90	43	43	86		27		41	41	83	44	45	89
F9c	68	4.07	6	9	15	6	7	13									
	32		39	46	85	44	43	87									
F9d	52	6.9	2	5	7	5	5	11									
	26		46	46	93	44	45	89									

Notes: The left (right) part of the table shows results for ferret (cat) data. The columns show (left to right): name of the data set (see Table 1), total number of singularities within the ROI, the number density ρ, and the percentages of nearest neighbors with the same and opposite sign (the first sign denotes the selected pinwheel, the second sign its nearest neighbor; $\sum$ denotes the sum for equal and opposite sign pairs) for experimental and for surrogate (SD) data.

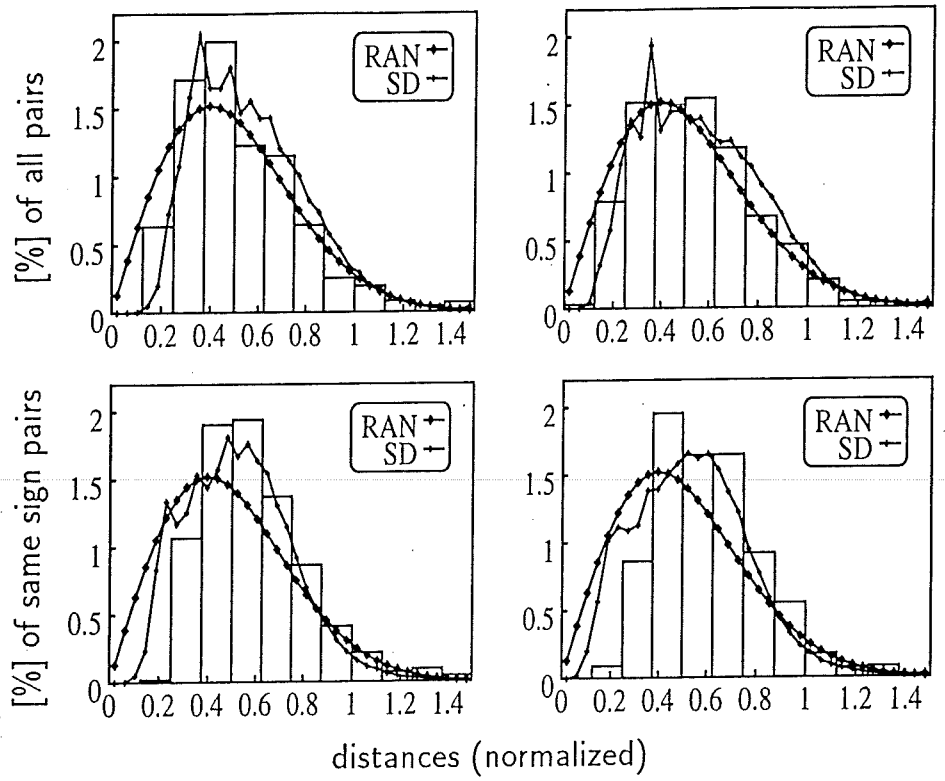

Figure 3: Percentage of pairs of singularities independent of sign (upper) as a function of their distance for ferret data (left) and for data from normally raised cats (right). All distances are normalized to the square root of the inverse number density of the singularities before averaging histograms over the different sets of data. Bins denote experimental data, diamonds the corresponding surrogate data maps (SD), and filled circles the results for a random distribution of points (RAN). The lower two plots show the distribution for same-sign singularities.

and ferrets. The distribution for surrogate data is shifted toward larger distances compared to the experimental data: 0.04Δ for ferrets and 0.03Δ for cats. Similar histograms have been constructed for all data sets and have been compared to the hypothesis random by a χ^2 test. Both the hypothesis RAN and the hypothesis SD have to be rejected for all sets of data ($\alpha = 0.05$). There were no obvious trends between different species and between animals of different ages. For the distribution of distances between nearest neighbors of the same sign and the opposite sign only, the shift to larger distances is more pronounced compared to pairs with opposite sign for both ferrets and cats (0.1Δ on average).

The results show the same tendency previously observed for primate orientation maps: that while singularities of opposite sign attract each other,

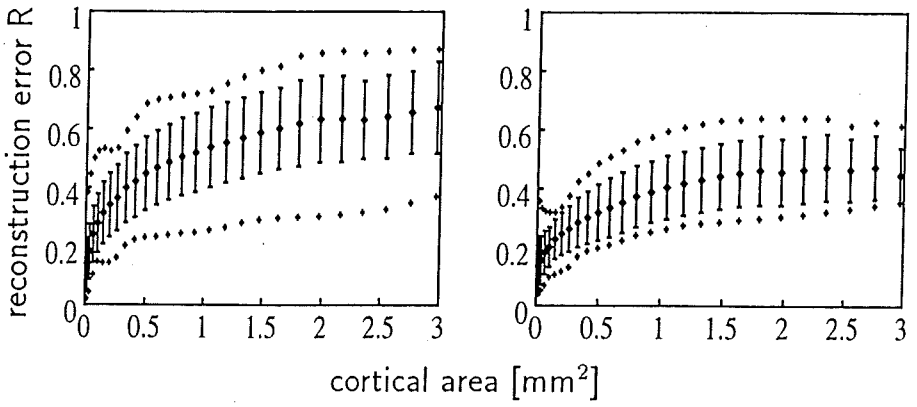

Figure 4: Average FAM reconstruction error as a function of region size for ferrets (left) and cats (right). The circles at the center of the vertical bars denote the average error over all data sets recorded with a low spatial resolution (no asterisks in Table 1), the bars denote the 2σ interval, and the outmost cross hairs denote the maximal and the minimal errors observed.

singularities on the whole repel themselves, compared to a random distribution. The sign correlations are of approximately equal strength in all three species; the shift of the distance distribution of distances is stronger in cat and macaque and less strong in ferret. The sign correlations are reproduced by surrogate data maps; however, sign correlations in those maps are significantly stronger than in the experimental maps. The distribution of distances between nearest neighbors, however, is well reproduced by the SD maps for cats and ferrets, in contrast to primates (Obermayer & Blasdel, 1997) for which the SD curve is shifted to larger distances.

4.3 Comparison of FAM Reconstructions with Data. Figure 4 shows the average reconstruction errors and their variation across all ferret (see Figure 4, left) and cat (see Figure 4, right) data sets as a function of the size of the reconstructed area. Reconstruction errors (see equation 3.3) are low for small areas and approach an average value of 0.5 (chance level is 0.907) for the largest maps. Reconstruction errors are on average smaller than the reconstruction errors previously obtained for primate maps (Obermayer & Blasdel, 1997); however, the size of the reconstructed area was considerably larger in that case, in μm as well as in units of Δ. FAM reconstructions of surrogate data maps show reconstruction errors, which are slightly less than the reconstruction errors of the original data.

4.4 Ocular Dominance Maps and Their Relationship with Orientation Preference Maps. Ocular dominance maps have been recorded from five sets of cat data, one of which is a longitudinal study from a stra-

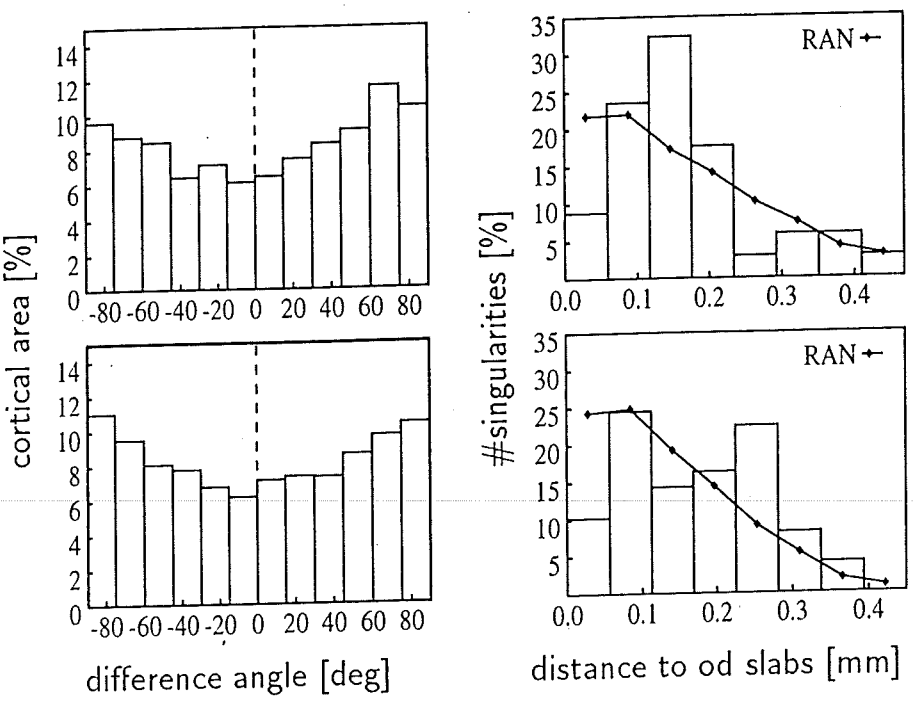

Figure 5: (Left) Percentage of cortical area as a function of the local intersection angle of the orientation and ocular dominance slabs for animal C7 (upper) and C8 (lower). Iso-orientation and iso-ocular dominance lines tend to cross each other orthogonally. (Right) Distributions of the smallest distances between orientation singularities and ocular dominance zero crossings for the same animals. Bins denote experimental data and diamonds the results for a random distribution of points (RAN). In contrast to the hypothesis RAN, singularities in experimental data significantly avoid very small distances to zero crossings, indicating their tendency to align along the ocular dominance centers (χ^2 test, significance level 30.7 > 12.6.

bismic kitten (CS1). The ocular dominance wavelengths, listed in Table 1, yield an average of 0.83 ± 0.06 mm for animals with ages between 50 and 61 days. For the longitudinal study (kitten CS1), the ocular dominance wavelength was found to increase with age by 0.8% per day (r = 0.74).

Gradients have been calculated for the orientation and the ocular dominance maps as described in the previous section. The cortical area is plotted against the angle of intersection between the orientation and the ocular dominance slabs in Figure 5 (left). Two of the three cats raised under normal conditions show a preference for orthogonality (Figure 5, left) (Hübener et al., 1997), whereas the two strabismic kittens do not. Singularities, however, tend to lie in the centers of the ocular dominance bands for all of the maps investigated (see Figure 4, right) (Hübener et al., 1997).

5 Discussion

5.1 Technical Considerations. Optical imaging of intrinsic signals implies two-dimensional neuronal activation patterns from the local changes in the blood oxygenation and the light-scattering properties of the tissue (Frostig, Lieke, Ts'o, & Grinvald, 1990; Bonhoeffer & Grinvald, 1996; Malonek & Grinvald, 1996) caused by active neuron populations. The total optical intrinsic signal represents a mixture of highly localized components, spatially more global yet stimulus-related components, and stimulus-independent components. In the context of optical imaging, the highly resolving components form the mapping signal, while the components with low spatial frequencies contribute to the biological noise. Because absorption and scattering of light in tissue strongly depend on the light wavelength, the relative sizes of the different components, the penetration depth from which the signals arise, and the effect of artifacts caused by superficial vasculature are functions of the light wavelength. At shorter wavelengths near 600 nm, intrinsic signals are dominated by the absorption behavior of hemoglobin, whereas at longer wavelengths beyond 700 nm, light-scattering effects increasingly dominate the intrinsic signals. Although a recent study (McLoughlin & Blasdel, 1997) has shown that the maps recorded with 720 nm and 605 nm do not differ much from each other, light at the shorter wavelength was found to be more strongly absorbed by the superficial blood vessels, which weakens the mapping signal. The wavelength used in this study yields scattering-dominated intrinsic signals.

Without further preprocessing, some of the measures addressed in this work, including the orientation histograms, singularity densities, and singularity locations, are affected by biological noise. In order to optimize the separation of mapping signals and biological noise, the singularity measures and the orientation histograms were calculated for different cutoff frequencies of the high-pass filters, and the common optimal value was chosen as the center of a plateau in the plot of the measures versus cutoff frequency. Although this method is probably unable to perform a complete separation of the components, it represents the optimal separation using bandpass filtering.

Our data sets were preprocessed by a normalization with a cocktail blank, which is the average of the recorded images over all stimulus conditions. This helps reduce the global components of the intrinsic signal (Bonhoeffer & Grinvald, 1996) and at the same time brings influences from all stimulus conditions into a single differential image. For example, if a differential image of horizontal and vertical orientations is divided by a cocktail blank, the resulting image implicitly contains contributions from the oblique orientations, because the cocktail blank does as well. Since this could affect the results of an analysis based on the latter images, we performed a second analysis of our orientation maps. This time we used frame analysis first and a subsequent subtraction of orthogonal single-condition stacks, but omit-

ted the normalization by a cocktail blank. The orientation histograms and the positions of the singularities were then compared with those obtained using a cocktail blank. The orientation histograms did not change significantly, and both versions were visually indistinguishable from each other. Also, the numbers of the singularities did not change, and their positions changed by one pixel at maximum. We conclude that normalization by the cocktail blank does not affect our results. A possible reason for this is that one major influence of the cocktail blank seems to be a reduction of the biological noise with low spatial frequency, which is subsequently removed again by bandpass filtering.

5.2 Statistical Significance and Comparison with Models. Ferret orientation maps showed a pronounced bimodal modulation caused by an overrepresentation of 0 degree and 90 degrees preferred orientations. The modulation of cat orientation histograms was only weak and not always confined to the 0 degree and 90 degrees orientation values. Statistical testing of these modulations against the hypothesis of a uniform distribution is difficult to perform, since the orientation values for neighboring pixels of the orientation map are not statistically independent. Correlations are introduced by both dependencies between the neuronal orientation preferences and a blur of the intrinsic signals of about 100 to 200 μm (Bonhoeffer & Grinvald, 1996) due to light scattering within the tissue (Stetter & Obermayer, 1999). We therefore considered the mean orientation taken over disjunct square patches with 125 μm in diameter (which is also the Nyquist frequency for the bandpass-filtered maps) to avoid statistical dependencies introduced by the blur, and performed the significance tests based on these samples.

The method used for the automatic detection of pinwheel centers evaluates the sum of orientations around closed pathways. Thus, it is directly related to the definition of singularities as sources of curl of a vector field. Because it evaluates only the sum over the orientations instead of requiring all orientations to be present around a singularity (Bonhoeffer, Kim, Malonek, Shoham, & Grinvald, 1995), the proposed method can also detect highly skewed singularities, around which orientations are strongly accumulated near some values. Other methods, which find singularities by detecting zeros of the complex orientation vectors (Löwel et al., 1998), again are sensitive to artifacts, if the zero crossing of the vector components meets at small angles, that is, if the singularities are highly skewed. The proposed method is insensitive against the skewness of singularities and in addition provides their signs. Accordingly, our results for the singularity densities, for example, $(3.5 \pm 0.2)\text{mm}^{-2}$ for cats, are somewhat higher than those found in the literature, which range between 2.1 and 2.7 mm^{-2} (Bonhoeffer et al., 1995; Löwel et al., 1998).

The comparison of orientation wavelengths and singularity densities between species and different deprivation stages was based on mean values and standard errors of the means over all animals of a given group.

This procedure neglects possible systematic interindividual variations of the quantities under considerations and treats maps from different animals as realizations of a single random process. However, this procedure provides an upper bound for the true error values, because the given errors now include both random and possible systematic contributions. As a consequence, findings that report quantities to be different from each other (singularity densities) can be regarded as significant; equality of data sets (in case of orientation wavelengths) could be spurious, because systematic interindividual variations can mask a small yet existing trend.

Orientation wavelengths and singularity densities are different in areas 17 and 18 (Bonhoeffer et al., 1995), and the cortical areas examined could possibly contain the 17/18 border and thus contain a small fraction of area 18. Hence, it cannot be ruled out a priori that our results are affected by contributions from area 18. We tested this point by subdividing the regions of interest for all data sets into a lateral and a medial part of equal size, such that one part could partially contain area 18, whereas the other part is purely area 17. We reanalyzed the orientation maps in both parts separately and compared the results with each other—once for individual animals and once for the sums over all animals. There was no statistically significant difference in the singularity densities, and the orientation wavelengths ranged within the general wavelength variability observed. One possible conclusion from this finding is that our data did not contain significant contributions of area 18. However, the areas and the total numbers of singularities in the subdivisions are rather small, which probably contributes to the lack of significance. However, one may conclude that based on the data available, our results are not significantly changed by the possible presence of small area 18 patches in the cortical area examined.

The distance and sign distributions of pairs of neighboring singularities were found to be significantly different from both the numbers predicted by the surrogate data (SD) and the two-dimensional Poisson (RAN) models. Real distributions showed less opposite sign pairs than SD data, and the singularities repelled each other compared to both SD and RAN, the latter trend being extraordinarily strong for same-sign singularity pairs. The positions of singularities can be affected by both random white noise and low-spatial frequency components of biological noise. The first contributions act to randomize the singularity distributions and thus tend to equalize the observed and the random singularity distributions. In particular, white noise cannot artificially generate the observed systematic deviations from a random distribution. Low spatial frequency noise in principle can cause systematic shifts in singularity positions. However, a close coincidence of singularity positions deduced from optical imaging with those obtained from tetrode measurements (Maldonado, Gödecke, Gray, & Bonhoeffer, 1997) shows that careful bandpass filtering can remove positional artifacts to a considerable degree. A significant difference of the measured singularity statistics to that predicted by the surrogate

data model (Swindale, 1982; Rojer & Schwartz, 1990) indicates that the hypothesis that orientation maps originate from spatial smoothing of random orientations has to be rejected and that higher than second-order statistics are important for the structural description of cat and ferret orientation maps.

The global structure of orientation maps between the singularities cannot be explained completely from an optimal smoothness criterion as implemented by field analogy models. The reconstruction error remains considerably below the error for random orientations, but increases systematically with the size of the map under consideration for both the measured and surrogate data. Therefore, the local behavior of orientation maps seems to follow an optimal smoothness criterion, while the global structure seems to show strong deviations from that principle. The drop of the error at very small map sizes is probably caused by smoothing due to both tissue scattering and the low-pass filter step during postprocessing. The relatively high reconstruction errors for larger maps can in part be caused by the neglect of anisotropies of the singularities (see also Obermayer & Blasdel, 1997, for monkey data).

5.3 Biological Implications. Our findings indicate that vertical and horizontal orientations are overrepresented in ferrets, whereas in cats only a weak tendency for overrepresentation is visible. One possible origin of overrepresentation is the more frequent occurrence of vertical and horizontal orientations of contrast lines in both artificial and purely natural visual scenes (Coppola, Purves, McCoy, & Purves, 1998; Field, 1987; van der Schaaf & van Hateren, 1996), which could have caused an overrepresentation of orientation preference during either ontogenetic or phylogenetic development.

The wavelengths of orientation maps in cat area 17 do not seem to change significantly between animals raised under normal conditions and strabismic animals of similar age. This finding gives rise to the hypothesis that the scale of the orientation map is only weakly dependent on the statistical structure of the visual input during development, and is mostly determined by factors intrinsic to the cortex, such as constraints based on the intrinsic cortical wiring patterns. It is consistent with the recent result that reverse occlusion during development leads to a precise restoration of the orientation map (Kim & Bonhoeffer, 1994; Gödecke & Bonhoeffer, 1996; Sengpiel et al., 1998), which also points toward the existence of intracortical factors determining the structures of orientation maps.

The singularity density has been found to decrease with age in one strabismic animal, while the ocular dominance wavelength increased. Wider ocular dominance bands have been reported for strabismic animals than for normal cats (Löwel, 1994). As both maps interact with each other, as, for example, demonstrated by the angular correlations between iso-orientation and iso-ocular dominance lines (see Figure 5), a structural change in the oc-

ular dominance pattern would be likely to evoke structural changes in the orientation map too. However, the observed increase in ocular dominance wavelength paralleled the isotropic growth of the primary visual cortex of cats during the same period (Sengpiel et al., 1998; Duffy, Murphy, & Jones, 1998).

The fact that across all animals included in this study, neither the orientation wavelengths nor the density of singularities were found to change significantly with age may be attributable to the fact that most of the ferret and cat data represented very limited age ranges (37 to 47 days and 50 to 60 days, respectively).

Acknowledgments

This work was funded by DFG (Ob 102/3-1), the Max-Planck-Gesellschaft, and the EC Biotech Program.

References

Anderson, P. A., Olavarria, J., & Sluyters, R. C. V. (1988). The overall pattern of ocular dominance bands in cat visual cortex. *J. Neurosci., 8,* 2183–2200.

Blasdel, G. G. (1992). Differential imaging of ocular dominance and orientation selectivity in monkey striate cortex. *J. Neurosci., 12,* 3115–3138.

Blasdel, G. G., & Salama, G. (1986) . Voltage-sensitive dyes reveal a modular organization in monkey striate cortex. *Nature, 321,* 579–585.

Bonhoeffer, T., & Grinvald, A. (1993). The layout of iso-orientation domains in area 18 of cat visual cortex: Optical imaging reveals a pinwheel-like organization. *J. Neurosci., 13,* 4157–4180.

Bonhoeffer, T., & Grinvald, A. (1996). Optical imaging based on intrinsic signals: The methodology. In A. Toga & J. C. Maziotta (Eds.), *Brain mapping: The methods* (pp. 55–97). Orlando, FL: Academic Press.

Bonhoeffer, T., Kim, D. S., Malonek, D., Shoham, D., & Grinvald, A. (1995). Optical imaging of the layout of functional domains in area 17 and across the area 17/18 border in cat visual cortex. *Eur. J. Neurosci., 7,* 1973–1988.

Chapman, B., & Bonhoeffer, T. (1998). Overrepresentation of horizontal and vertical orientation preferences in developing ferret area 17. *Proc. Natl. Acad. Sci. USA, 95,* 2609–2614.

Chapman, B., Stryker, M. P., & Bonhoeffer, T. (1996). Development of orientation preference maps in ferret primary visual cortex. *J. Neurosci., 16,* 6443–6453.

Coppola, D. M., Purves, H. R., McCoy, A. N., & Purves, D. (1998). The distribution of oriented contours in the real world. *Proc. Natl. Acad. Sci., 95,* 4002–4006.

Coppola, D. M., White, L. E., Fitzpatrick, D., & Purves, D. (1998). Unequal representation of cardinal and oblique contours in ferret visual cortex. *Proc. Natl. Acad. Sci., 95,* 2621–2623.

Cowan, J. & Friedman, A. (1991). Simple spin models for the development of ocular dominance columns and iso-orientation patches. In R. Lippman,

J. Moody, & D. Touretzky (Eds.), *Advances in neural information processing systems, 3* (pp. 26–31). San Mateo, CA: Morgan Kaufmann.

Duffy, K. R., Murphy, K. M., & Jones., D. G. (1998). Analysis of the postnatal growth of visual cortex. *Vis. Neurosci., 15*, 831–839.

Erwin, E., Obermayer, K., & Schulten, K. (1995). Models of orientation and ocular dominance columns in the visual cortex: A critical comparison. *Neural Comput., 7*, 425–468.

Field, D. J. (1987). Relations between the statistics of natural images and the response properties of cortical cells. *J. Opt. Soc. Am. A, 4*(12), 2379–2394.

Freund, I. (1994). Optical vortices in gaussian random fields: Statistical probability densities. *J. Opt. Soc. Am. A, 11*, 1644–1652.

Frostig, R. D., Lieke, E. E., Ts'o, D. Y., & Grinvald, A. (1990). Cortical functional architecture and local coupling between neuronal activity and the microcirculation revealed by in vivo high-resolution optical imaging of intrinsic signals. *Proc. Natl. Acad. Sci USA, 87*, 6082–6086.

Gödecke, I., & Bonhoeffer, T. (1996). Development of identical orientation maps for two eyes without common visual experience. *Nature, 379*, 251–254.

Hübener, M., Shoham, D., Grinvald, A., & Bonhoeffer, T. (1997). Spatial relationships among three columnar systems in cat area 17. *J. Neurosci., 17*, 9270–9284.

Kim, D. S., & Bonhoeffer, T. (1994). Reverse occlusion leads to a precise restoration of orientation preference maps in visual cortex. *Nature, 370*, 370–372.

LeVay, S., Stryker, M. P., & Shatz, C. J. (1978) . Ocular dominance columns and their development in layer IV of the cat's visual cortex: A quantitative study. *J. Comp. Neur., 179*, 223–244.

Löwel, S. (1994). Ocular dominance column development: Strabismus changes the spacing of adjacent columns in cat visual cortex. *J. Neurosci., 14*, 7451–7468.

Löwel, S., Schmidt, K. E., Kim, D. S., Wolf, F., Hoffsmmer, F., Singer, W., & Bonhoeffer, T. (1998). The layout of orientation and ocular dominance domains in area 17 of strabismic cats. *Europ. J. Neurosci., 10*, 2629–2643.

Maldonado, P. E., Gödecke, I., Gray, C. M., & Bonhoeffer, T. (1997). Orientation selectivity in pinwheel centers in cat striate cortex. *Science, 276*, 1551–1555.

Malonek, D., & Grinvald, A. (1996). Interactions between electrical activity and cortical microcirculation revealed by imaging spectroscopy: Implications for functional brain mapping. *Science, 272*, 551–554.

McLoughlin, N. P., & Blasdel, G. G. (1997). Effect of wavelength on differential images of ocular dominance and orientation in monkey striate cortex. *Soc. Neurosci. Abstr., 23*, 13.

Niebur, E., & Wörgötter, F. (1994). Design principles of columnar organization in visual cortex. *Neural Comput., 6*, 602–614.

Obermayer, K., & Blasdel, G. G. (1993). Geometry of orientation and ocular dominance columns in monkey striate cortex. *J. Neurosci., 13*, 4114–4129.

Obermayer, K., & Blasdel, G. G. (1997). Singularities in primate orientation maps. *Neural Comput., 9*, 555–567.

Papoulis, A. (1965). *Probability, random variables, and stochastic processes*. New York: McGraw-Hill.

Redies, C., Diksic, M., & Riml, H. (1990). Functional organization in the ferret visual cortex: A double-label2-deoxyglucose study. *J. Neurosci., 10,* 2791–2803.

Rojer, A. S., & Schwartz, E. L. (1990). Cat and monkey cortical columnar pattern modeled by bandpass-filtered 2D white noise. *Biol. Cybern., 62,* 381–391.

Schwartz, E. L. (1994). Computational studies of the spatial architecture of primate visual cortex. In A. Peters & K. S. Rockland (Eds.), *Cerebral cortex.* New York: Plenum Press.

Sengpiel, F., Gödecke, I., Strawinski, P., Hübener, M., Löwel, S., & Bonhoeffer, T. (1998). Innate and environmental factors in the formation of functional maps in cat visual cortex. *Neuropharmacology, 37,* 607–621.

Shmuel, A., & Grinvald, A. (1996). Functional organization for direction of motion and its relationship to orientation maps in cat area 18. *J. Neurosci., 16,* 6945–6964.

Shvartsman, N., & Freund, I. (1994). Vortices in random wave fields: Nearest neighbor anticorrelations. *Phys. Rev. Lett., 72,* 1008–1011.

Spiegel, M. R. (1975). *Probability and statistics.* New York: McGraw-Hill.

Stetter, M., & Obermayer, K. (1999). Simulation of scanning laser techniques for optical imaging of blood-related intrinsic signals. *J. Opt. Soc. Am. A, 16,* 58–70.

Swindale, N. V. (1982). A model for the formation of orientation columns. *Proc. R. Soc. Lond. B, 215,* 211–230.

van der Schaaf, A., & van Hateren, J. H. (1996). Modelling the power spectra of natural images: Statistics and information. *Vision Res., 36,* 2759–2770.

Weliky, M., Bosking, W. H., & Fitzpatrick, D. (1996). A systematic map of direction preference in primary visual cortex. *Nature, 379,* 725–728.

Wolf, F., Pawelzik, K., & Geisel, T. (1994). Emergence of long-range order in maps of orientation preference. In M. Marinaro & P. G. Morasso (Eds.), *Artificial neural networks I.* Amsterdam Elsevier Science.

Wolf, F., Pawelzik, K., Geisel, T., Kim, D. S., & Bonhoeffer, T. (1994). Optimal smoothness of orientation preference maps. In F. H. Eeckman (Ed.), *Computation in neurons and neural systems.* Norwell, MA: Kluwer.

Received February 17, 1999; accepted February 15, 2000.